Geomechanics and Engineering, *Vol. 38, No. 5 (2024) 517-528*
https://doi.org/10.12989/gae.2024.38.5.517

Investigation of pile group response to adjacent twin tunnel excavation utilizing machine learning

Su-Bin Kim[1a], Dong-Wook Oh[2b], Hyeon-Jun Cho[1c] and Yong-Joo Lee*[1]

[1]*Department of Civil Engineering, Seoul National University of Science and Technology, 232 Gongneung-ro, Nowon-gu, Seoul, 139-743, Republic of Korea*
[2]*Department of Railroad Construction and Safety Engineering, Dongyang University, 145 Dongyangdaero Punggi-eup, Yeongju-si 36040, Republic of Korea*

(*Received December 4, 2023, Revised January 24, 2024, Accepted February 2, 2024*)

Abstract. For numerous tunnelling projects implemented in urban areas due to limited space, it is crucial to take into account the interaction between the foundation, ground, and tunnel. In predicting the deformation of piled foundations and the ground during twin tunnel excavation, it is essential to consider various factors. Therefore, this study derived a prediction model for pile group settlement using machine learning to analyze the importance of various factors that determine the settlement of piled foundations during twin tunnelling. Laboratory model tests and numerical analysis were utilized as input data for machine learning. The influence of each independent variable on the prediction model was analyzed. Machine learning techniques such as data preprocessing, feature engineering, and hyperparameter tuning were used to improve the performance of the prediction model. Machine learning models, employing Random Forest (RF), eXtreme Gradient Boosting (XGB), and Light Gradient Boosting Machine (LightGBM, LGB) algorithms, demonstrate enhanced performance after hyperparameter tuning, particularly with LGB achieving an R^2 of 0.9782 and RMSE value of 0.0314. The feature importance in the prediction models was analyzed and P_N was the highest at 65.04% for RF, 64.81% for XGB, and P_{CTC} (distance between the center of piles) was the highest at 31.32% for LGB. SHAP was utilized for analyzing the impact of each variable. P_N (the number of piles) consistently exerted the most influence on the prediction of pile group settlement across all models. The results from both laboratory model tests and numerical analysis revealed a reduction in ground displacement with varying pillar spacing in twin tunnels. However, upon further investigation through machine learning with additional variables, it was found that the number of piles has the most significant impact on ground displacement. Nevertheless, as this study is based on laboratory model testing, further research considering real field conditions is necessary. This study contributes to a better understanding of the complex interactions inherent in twin tunnelling projects and provides a reliable tool for predicting pile group settlement in such scenarios.

Keywords: machine learning; numerical analysis; pile group; pile group-tunnel interaction; twin tunnelling

1. Introduction

In recent years, many tunnelling projects have been implemented due to the limited space available for infrastructure in urban areas. This involves the construction of new tunnels near existing tunnels or the construction of twin tunnels in close proximity to each other. The urban underground is congested with the foundations of skyscrapers and tunnels of various sizes. Furthermore, tunnelling inevitably causes some ground movement and changes in ground stress, potentially adversely affecting nearby structures.

Various studies have been conducted to investigate the effects of urban tunnelling on existing pile foundations (Mroueh and Shahrour 2002, Xiang and Feng 2013, Marshall and Haji 2015, Heama *et al*. 2017, Jung *et al.* 2022, Jeon and Lee 2023) and the mechanisms for the deformation of the ground induced by twin tunnelling (Choi and Lee 2010, Chakeri *et al.* 2011, Fang *et al.* 2015, Do *et al.* 2016, Hong *et al.* 2020, Ahn *et al.* 2022, Liu *et al.* 2022).

According to Ayasrah *et al.* (2021), numerical simulations were performed to investigate the impact of the construction of the Greater Cairo Metro tunnel on the pile cap foundation of an adjacent Attaba building. Several parameters were investigated, such as tunnel diameter, distance between piles and tunnel, and tunnel depth. The analysis revealed that tunnelling induces additional axial forces and bending moments and increases axial settlement and lateral deflection. Tunnel depth and diameter were found to have a highly significant effect on the pile response. Kong *et al.* (2017) investigated the behaviour of embedded piles and surrounding ground due to tunnelling in soft ground. The settlement of the piles and the ground and the axial force of the embedded piles due to the offset between the pile toe and the tunnel crown were analyzed through model tests and 3D FEM analysis. The study indicated that settlement increases when the offset between the pile toe and the tunnel decreases.

*Corresponding author, Professor
E-mail: ucesyjl@seoultech.ac.kr
[a]Ph.D. Student
[b]Ph.D.
[c]M.S. Student

ISSN: 2005-307X (Print), 2092-6219 (Online)

Chu *et al.* (2007) conducted a model test and a two-dimensional numerical simulation of a circular twin tunnel with a multilayer structure. As a result, the initial stress that causes tunnel failure increases with K, which shows that the stability of the twin tunnel is improved when the direction of the major principal stress is parallel to the alignment direction of the twin tunnel. Mirhabibi and Soroush (2012) analyzed the two-dimensional numerical model using field data and ABAQUS software and considered the important parametric influences such as tunnel depth, tunnel center-to-center distance, and building stiffness. They also presented graphs to estimate the maximum settlement of the building by applying a correction factor to the greenfield settlement during the preliminary design phase.

While numerous studies have investigated the effects of tunnelling on existing piles, often only a single tunnel excavation is considered. Research on the effects of twin tunnelling on existing piles is relatively scarce. Ng *et al.* (2013) conducted a series of three-dimensional centrifugal model tests to investigate the effects of twin tunnelling on existing single piles. Twin tunnels were excavated near the piles to investigate the influence at different tunnel depths. The pile settlement induced by tunnelling near the toe was found to be approximately 2.2 times greater than that caused by tunnelling in the middle of the pile. Ng and Lu (2014) investigated the effect of the construction sequence of twin tunnels on existing piles through a series of 3D centrifuge model tests and numerical analyses. The settlement was found to be approximately 33% greater for the sequence of tunnelling near the toe of the pile followed by tunnelling near the mid-depth of the pile than for the reverse sequence, which induced a greater reduction in pile end-bearing capacity and skin friction.

In geotechnical engineering, as well as in piling (foundations) and tunnelling, one may face highly complex and not fully understood problems. This is because geotechnical engineering deals with the physical behaviour of materials (sand, clay, rock, etc.) that are inherently diverse and face uncertainties. Researchers and engineers have simulated the complex behaviour of geotechnical problems through numerical analysis, laboratory model testing, and field experiments to analyze and predict dynamic behaviours, such as the deformation and failure mechanisms of the ground. Additionally, over the past two decades, artificial intelligence has been applied to geotechnical engineering to solve complex engineering problems. Recent studies have actively applied various algorithms beyond Artificial Neural Networks (ANN) in geotechnical engineering (Sou-Sen and Chuang 2004, Nejad *et al.* 2009, Gordan *et al.* 2019, Alseid *et al.* 2023, Han *et al.* 2023, Oh *et al.* 2023).

Kim *et al.* (2001) combined field monitoring results with ANN to predict settlement for a tunnel construction site. The optimal neural network model was proposed through a preliminary parametric study, and a sensitivity test was performed using RSE. Overall, the most sensitive factors affecting settlement due to tunnelling were found to be tunnel depth, tunnel excavation depth, groundwater level, inflow volume, rock type, and excavation rate. Oh *et al.* (2021) developed a model that utilizes machine learning

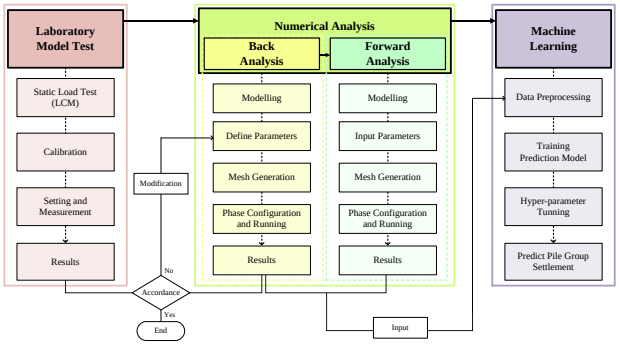

Fig. 1 Flow chart of this study

to predict settlement by distinguishing between the raft and piles of a piled raft foundation, and to predict the rate of change of settlement along the length of the piles. The results of laboratory model tests and three-dimensional numerical analysis were used as a database for machine learning, and the XGB algorithm was used to quantitatively analyze the characteristics that affect the prediction model. Among the features, the horizontal offset between the pile and tunnel exerted the most significant influence, while the pile diameter and number of piles had relatively small effects.

In this study, the behaviour of the pile group was investigated when the twin tunnel was excavated under the existing pile group foundation. Finite element numerical back-analysis was performed based on laboratory model test results. The data obtained through the numerical analysis was used as input data to the machine learning prediction model to predict the settlement of the pile group. The overall flow of this study is shown in Fig. 1.

2. Laboratory model test

2.1 Model test simulation procedure

The actual ground behaviour induced by tunnel excavation is three-dimensional. However, in this experiment, scaled model testing was conducted under two-dimensional plane-strain conditions. One significant drawback of scaled model testing is the inability to simulate the actual stress in the ground. Although there are centrifuge model tests that can overcome this limitation, they are often constrained by high costs and difficulties in preparation, installation of measurement instruments, and other factors, relative to the time spent on experiments. Therefore, to carry out this study, a laboratory model test was performed under 2D plane-strain conditions considering a scale of 1/100 based on the tunnel diameter (D). A model chamber (Fig. 2(a)) with dimensions of 1500 mm×700 mm×100 mm was constructed with acrylic panels on the front and back sides to facilitate observation and photography of the ground deformation. A pile group model (Fig. 2(b)) was constructed with a two-dimensional cross-section that is equivalent to the original shape cross-section under plane strain conditions when the piles in a row are closely spaced (Potts 2001). To prevent eccentric loading on the pile group,

(a) Model test chamber

(b) Pile group model

(c) Tunnel model

(d) Hydraulic pump

Fig. 2 Equipment for laboratory model test

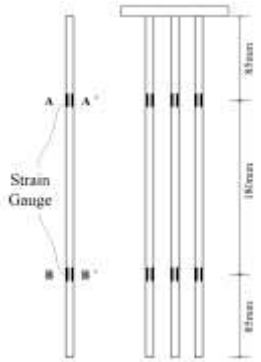

Fig. 3 Pile group model with strain gauge positions

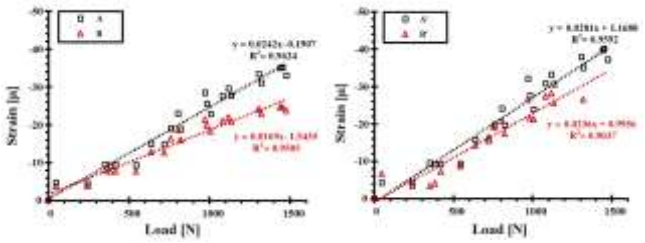

(a) Top part (b) Bottom part

Fig. 4 Results of strain gauge calibration

a pile cap was installed at a distance above the ground surface, eliminating the need to account for the raft effect of the pile. To simulate the twin tunnelling, a model tunnel with a diameter of 100mm (Fig. 2(c)) was created, and a membrane was used in combination with the model tunnel. To simulate tunnel excavation, the concept of volume loss was applied, and water was pumped into the model tunnel and extracted by a hydraulic pump (Fig. 2(d)) to simulate tunnel excavation.

As shown in Fig. 3, the strain gauges were attached to the pile group model to verify the distribution of axial force generated in the pile group foundation due to twin tunnel excavation. In order to improve the precision of the axial force generated by the pile, a calibration test was performed to calculate the axial force through the strain measured by the strain gauge. A Universal Testing Machine (UTM) was employed to establish the relationship between strain and axial force generated in the pile group model, and the strain-load relationship curve (Fig. 4) was derived by measuring the strain induced by incremental loading. The linear relationship equation between strain and load obtained through linear regression analysis is summarized in Table 1, with R^2 values ranging from 0.9037 to 0.9624, indicating a high degree of reliability. The results of measuring axial forces by attaching strain gauges to piles were conducted as an indicator to understand trends for finding soil properties in laboratory model tests.

The relationship between water volume and tunnel diameter to simulate the volume loss rate during tunnel excavation was determined based on Kong et al. (2016). The stage of the calibration test was performed by increasing the volume loss rate to 40% to simulate the ground failure caused by tunnel excavation. To calculate the allowable load of a pile model, a static test based on the Load Control Method (LCM) was performed. The static

Table 1 Linear equations for each strain gauge

Part	Linear Equation	Reliability
A	y = - 0.024x - 0.19	R^2 = 0.96
B	y = - 0.016x - 1.54	R^2 = 0.95
A'	y = - 0.028x + 1.17	R^2 = 0.96
B'	y = - 0.023x + 0.99	R^2 = 0.90

* y = load(N), x = strain(μ)

pile load test was performed to measure the settlement of the pile with respect to the load using Linear Variable Differential Transformers (LVDT) and then determining the load-settlement relationship curve (P-S curve).

Standard sand from Jumunjin was placed in a sand pouring device (Fig. 2(a)) was employed to maintain a constant sand distribution to the ground surface, creating a homogeneous sandy soil subgrade. The interaction between the soil-pile-structure is influenced by the relative density of the soil. The relative density of the soil is a crucial factor, as changes in it result in variations in confinement pressure and soil stiffness, thereby affecting the overall behavior of the system. Therefore, the relative density of the sandy soil was calculated by installing moisture content cans at 250mm intervals from the bottom of the model test chamber (Kim *et al.* 2012). The soil formed with an average relative density of 33.5%, and was classified as loose soil according to the soil classification criteria based on the relative density of sandy soil (Das 2011). Fig. 5 is a schematic diagram showing the detailed structure of the laboratory model test. The experimental setup, configured in accordance with the schematic diagram and equipment in Fig. 2, was employed to conduct the experiments. Two model tunnels (Fig. 2(c)) were installed at a distance of the

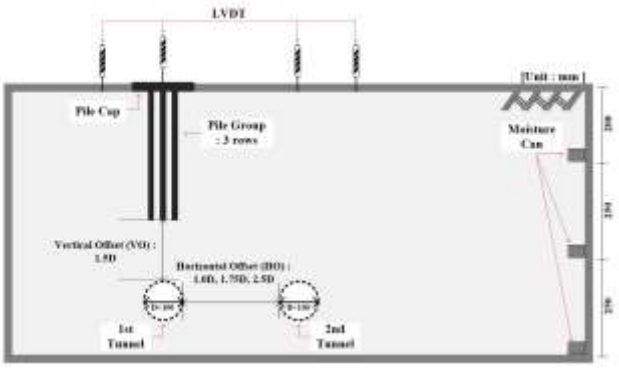

Fig. 5 Schematic diagram of laboratory model test

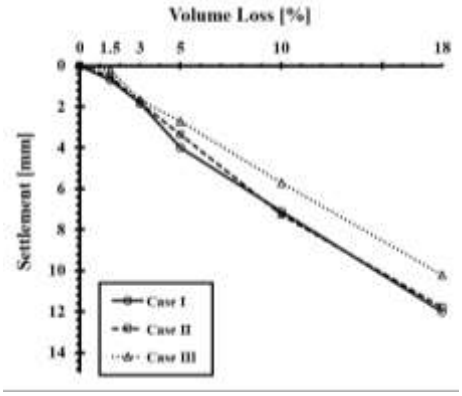

Fig. 6 Pile cap settlements for laboratory model test

tunnel diameter (D) away from the bottom of the model chamber (Fig. 2(a)), assuming the floor of the model chamber floor as the bedrock. To simulate twin tunnel excavation, the spacing between the pillar of the two tunnels was varied in three cases: 1.0D, 1.75D, and 2.5D (Table 2). The pile group was installed to be 1.5D vertically offset from the first tunnel's crown, and the settlement of the pile group and the ground surface was measured using Linear Variable Differential Transducers (LVDT).

2.2 Results of laboratory model test

The results of the settlement measured on the center of the pile cap by using LVDTs in the laboratory model tests are presented in Fig. 6. For the 1st tunnel, the excavation was simulated using the general soft ground volume loss rate of 1.5%. For the 2nd tunnel, the volume loss rate was incrementally increased in five stages (1.5%, 3%, 5%, 10%, 18%) to simulate progressive damage. Among these, only the results obtained with a volume loss rate of 1.5 are used in numerical analysis.

The settlement at the pile cap during the first tunnel excavation was 0.261 mm, 0.196 mm, and 0.102 mm in Case I, respectively. Similarly, for the second tunnel excavation, Case I had the largest settlement of 0.69 mm, followed by Case II and Case III with 0.53 mm and 0.196 mm, respectively. In general, the greater distance between tunnels tended to result in smaller settlements. In Case I, settlements were 30.2% and 252.1% larger than in Case II and Case III, respectively.

Regarding the axial force of the piles, only the results of the right-side pile were highlighted during the second tunnelling. The positive (+) values on the x-axis represent tension in the pile, while negative (-) values represent compression. The y-axis normalizes the position of the strain gauge relative to the length of the pile, with a y/L of 0 near the pile toe and 1 near the pile head.

The distribution of axial forces acting on the piles due to the twin tunnel excavation is shown in Fig. 7. Overall, the pile head experienced compression, while the pile toe experienced tension. During the first tunnel excavation, the left pile toe showed tension forces of 110.7N, 103.9N, and 121.2N for each case, and the left pile head showed compression forces of -10.0N, -22.3N, and -16.5N, respectively. The right pile toe showed tension forces of

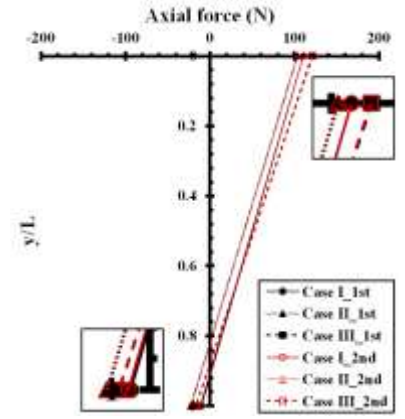

(a) Left side on pile group

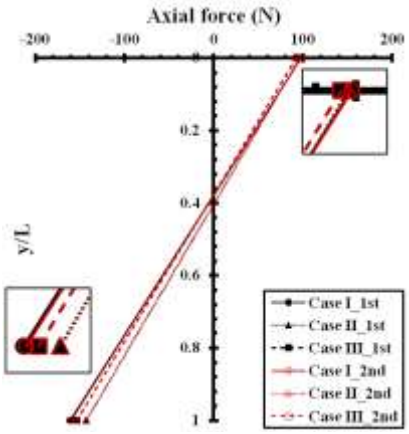

(b) Right side on pile group

Fig. 7 Axial forces in laboratory model test

Table 2 Summary of cases

Case	Number of piles	Vertical offset	Horizontal offset
Case I	3	1.5D	1.0D
Case II			1.75D
Case III			2.5D

97.8N, 96.2N, and 92.5N, and the right pile head showed compression forces of -161.3N, -143.1N, and -153.6N, respectively. It can be seen that the left side of the pile is dominated by tension rather than compression, while the

Table 3 Material properties for numerical analysis

Material	Symbol	Unit	Loose sand	Medium Sand	Dense Sand	Pile
Unit weight	γ	kN/m^3	17	18	19	-
Young's modulus	E	kPa	20,000	40,000	50,000	24,500,000
Poisson's ratio	υ	-	0.3	0.3	0.3	0.25
Cohesion	c	kPa	0	0	0	-
Shear resistance angle	φ	° (deg)	30	35	40	-
Dilatancy angle	ψ	° (deg)	5	5	10	-
R_{inter}	-	-	0.8	0.7	0.5	-

*R_{inter}: The strength reduction factor is applied to the interfaces between all of the models and the ground (PLAXIS 2023)

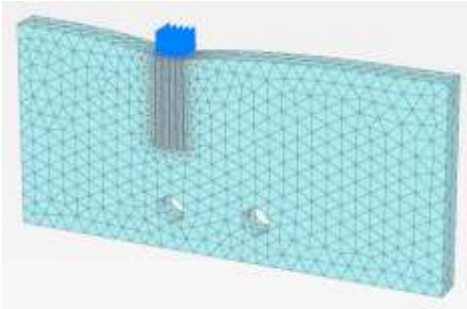

Fig. 8 Mesh generation

right side of the pile experienced relatively more compression than tension.

The distribution of axial forces on the pile during the second tunnelling followed a similar trend to the first tunnelling. On the left side, axial forces of up to 120.8N and -24.5N were measured at the toe and head of the pile, respectively. Axial forces of up to 98.6N and -159.9N were measured at the pile toe and head of the right side of the pile, respectively. The cause of the tensile force at the toe of the pile is estimated as a result of loss of ground due to tunnel excavation. In most cases, the tensile force at the pile toe decreased as the tunnel distance increased.

3. Numerical analysis

This study utilized PLAXIS 2D and 3D, a numerical analysis program based on the finite element method. This chapter delves into the three-dimensional numerical modelling and pile settlement results necessary for the machine learning database. Numerical analysis was performed using the inverse method (back analysis) to obtain the material properties of the target ground based on the measurements of the laboratory model test, and 918 deterministic calculations were performed with the numerical analysis automation program (forward analysis) for the machine learning database.

3.1 Modelling and material properties

For the finite element numerical modelling, the Mohr-Coulomb model was applied to the soil, while a linear elastic model was used for the piled foundation. The modulus of elasticity of the ground was simulated based on the relative density of the soil, and the material properties required for each modelling were referenced from established literature by (Lambe and Whitman 1979, Das 2011), considering typical sandy soil conditions. The properties and units applied to the soil and pile are summarized in Table 3.

It should be noted that the groundwater level was not considered and all sizes were modelled based on the laboratory model tests in the analysis. Although the size is not optimal for 3D analysis, it was used to estimate the properties of the ground through inverse analysis. The estimated soil properties of the indoor model test ground through inverse analysis are presented in Table 4.

The variables considered in the numerical analysis include the elastic modulus of the ground, pile diameter, pile length, number of piles, pile center-to-center distance (pile spacing), and tunnel center-to-center distance (tunnel spacing). The ranges of application for each variable are summarized in Table 5. The pile diameter, length, and spacing were determined based on the Design Criteria for Structure Foundation (Korean Geotechnical Society 2016).

The numerical simulation considered the following procedure: excavation, pile driving, pile loading, excavation of the first tunnel, completion of the first tunnel construction, and excavation of the second tunnel. Tunnel excavation was simulated by introducing the concept of volume loss in the ground. Since this study focuses on the behaviour of the twin tunnels excavated under existing pile foundations in urban areas, the effects of the sequence of construction steps are not considered. The mesh generation for the numerical analysis is shown below in Fig. 8.

3.2 Results of numerical analysis

This study was conducted to investigate ground behaviour based on the spacing of the twin tunnel in urban areas, and trends were observed through both model tests and numerical analysis. The pile group settlement results obtained from the numerical analysis conducted in this study are presented in Fig. 9. Fig. 9(a) shows the results of E_{ref} and pile group settlement decreases as E_{ref} increases. In general, when designing pile group, pile group settlement tends to decrease as the number, length, and diameter of piles increase. However, in this study, the settlement

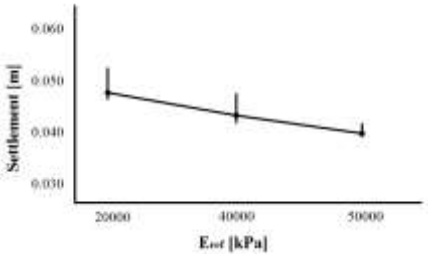

(a) Settlement for E_{ref}

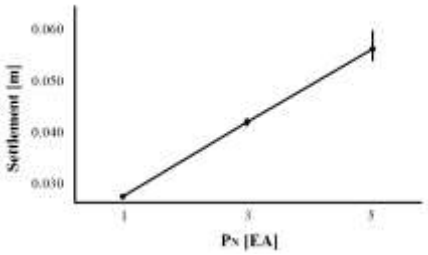

(b) Settlement for P_N

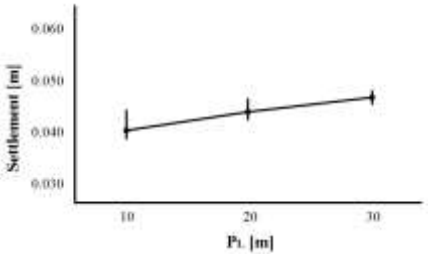

(c) Settlement for P_L

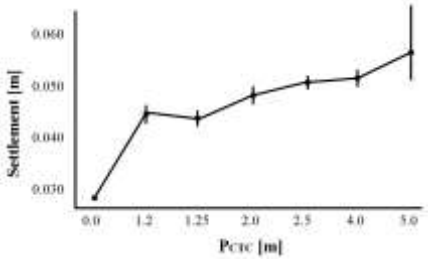

(d) Settlement for P_{CTC}

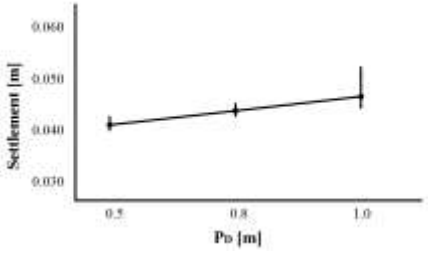

(e) Settlement for P_D

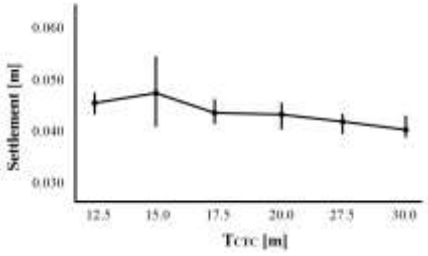

(f) Settlement for T_{CTC}

Fig. 9 Results from numerical analysis

Table 4 Estimated material properties of model test through inverse analysis

Material	Symbol	Unit	Loose sand
Unit weight	γ	kN/m^3	14.14
Young's modulus	E	kPa	22,150
Poisson's ratio	υ	-	0.34
Cohesion	c	kPa	0
Shear resistance angle	φ	°(deg)	30
Dilatancy angle	ψ	° (deg)	0
R_{inter}	-	-	0.8

increases as the number of piles, length, spacing, and diameter increase, as shown in Figs. 9(b)-9(e). This is because the load was applied to the pile group by varying the size of the load according to the design variables of the pile group, and the raft effect of the pile group was not considered. As the pile spacing increases, the vertical load transmitted to the ground by each pile is distributed and the bearing capacity of the pile group decreases. Therefore, as shown in Fig. 9(d), as the pile spacing increases, the settlement of the pile group rises, attributed to the reduction in the bearing capacity of the pile group. Fig. 9(f) illustrates the results of T_{CTC} and pile group settlement, showing a decreasing trend in pile group settlement as the tunnel spacing increases. It should be noted that Fig. 9 represents the average values of pile group settlement according to each variable, and it is difficult to identify the correlation with other variables in the numerical analysis where various factors are considered comprehensively.

4. Prediction model for pile group Settlement

4.1 Data acquisition and preprocessing

In this study, a prediction model was derived and optimized using various variables and algorithms to predict the settlement of the pile group when the twin tunnel is constructed adjacent to the pile group. The overall flow of machine learning attempted in this study is summarized in Fig. 10.

The variables considered in the numerical analysis are utilized as input data for machine learning. A total of 918 datasets were collected, and Fig. 11 shows that there are no missing values in the input data. Removing all missing values may lead to data loss, and incorrect replacement can result in data bias. Therefore, handling missing values is a crucial step in data preprocessing, as they can be disruptive factors in data analysis.

The correlation results among the variables are summarized in Fig. 12. Correlation indicates a linear relationship between two variables. Correlation does not imply causation and a high correlation does not mean that one variable explains the cause of the other variable. Correlations closer to 0 indicate no proportional relationship, those closer to -1 indicate a strong negative

Table 5 Feature conditions for numerical analysis

Feature acronym	Definition	Units	Ranges
E_{ref}	Relative soil density	kPa	20e3, 40e3, 50e3
P_N	Number of piles	m	1, 3, 5
P_L	Pile length	m	10, 20, 30
P_{CTC}	Distance between center of piles (d = pile diameter)	m	0.0d, 1.2d, 2.5d, 5.0d
P_D	Pile diameter	m	0.5, 0.8, 1.0
T_{CTC}	Distance between center of tunnels (D = tunnel diameter)	m	1.25D, 1.5D, 1.75D, 2D, 2.75D, 3D

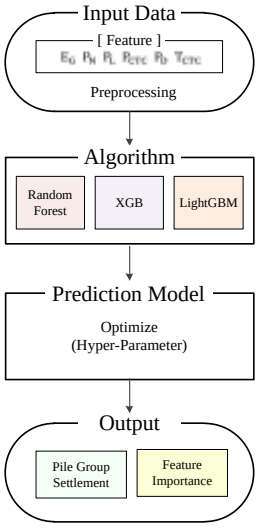

Fig. 10 Flow chart of machine learning procedure

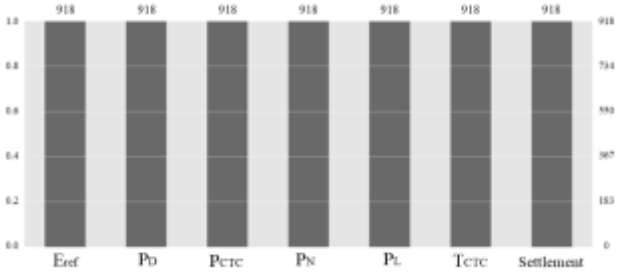

Fig. 11 Null checking for input data

correlation, and those closer to 1 indicate a strong positive correlation. The most correlated variable with the target variable, settlement, is P_N with a correlation of 0.537, meaning that a larger P_N value corresponds to a larger pile group settlement. The least correlated variable with pile group settlement is T_{CTC} with a value of 0.087, and the smaller the T_{CTC} value, the greater the pile group settlement.

To evaluate the performance of the model and prevent overfitting, the entire dataset was split into training, validation, and test data sets in a ratio of 5:3:2. In addition, data was normalized and standardized to simplify the units and ranges of the features. Normalization used scikit-learn's MinMaxScaler to transform the scale of values to be between 0 and 1, while standardization used scikit-learn's StandardScaler to change the range of values to have a mean of 0 and a variance of 1.

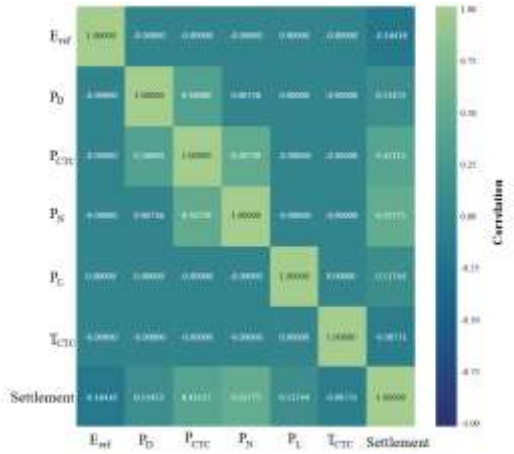

Fig. 12 Feature correlations

4.2 Building prediction model

4.2.1 Algorithm selection process

RF is an ensemble learning method widely used for classification and regression analyses. It is an algorithm that works by outputting classification or regression analysis from multiple decision trees constructed during training. It is applicable to both classification and regression problems, easy to handle missing values, and effective for processing large datasets. Additionally, it has the advantage of easy parameter adjustment and mitigates the overfitting problem, enhancing model accuracy. However, due to the nature of RF, forming hundreds to thousands of trees in proportion to the data size, it takes a long time for predictions, and analyzing individual trees is challenging as not all generated tree models can be examined.

XGB is another powerful tree-based algorithm widely used in machine learning. Similar to RF, it employs a tree-based ensemble learning method. XGB operates with parallel processing, ensuring fast learning and classification speeds. It utilizes regularization and shrinkage techniques to control model complexity and prevent overfitting. However, like other tree models, XGB can only predict values within the train data and does not support distributed processing. It provides a range of hyperparameters for model adjustment, but it depends on the skill of the analyst to effectively combine the hyperparameters to build an optimal model.

LGB is a gradient-boosting framework designed for large-scale and distributed learning. It offers optimized algorithms for fast learning and low memory usage. Unlike

Table 6 Performance metrics for the training data of each algorithm

Indicator	Random Forest		XGBoost		LightGBM	
	Normalization	Standardization	Normalization	Standardization	Normalization	Standardization
R^2	-21.5108	0.9627	-9.2983	0.0469	-139.1805	0.5550
MAE	0.3601	0.0641	0.3663	0.3542	0.3632	0.1650
MSE	0.1665	0.0067	0.1700	6.1864	0.1670	0.2055
RMSE	0.4081	0.0817	0.4123	2.4872	0.4086	0.4533

Table 7 R^2 and RMSE values depending on hyperparameter tuning

Indicator		Random Forest		XGBoost		LightGBM	
		Before	After	Before	After	Before	After
R^2	Nom.	-21.5108	0.9390	-9.2983	0.9456	-139.1805	0.9782
	Std.	0.9627	0.7265	0.0469	0.1268	0.5550	0.1670
RMSE	Nom.	0.4081	0.0520	0.4123	0.0505	0.1670	0.0314
	Std.	0.0817	0.2196	2.4872	0.2468	0.4533	0.2344

Table 8 Hyper-parameters for each algorithm

Random Forest		XGBoost		LightGBM	
Hyper-Parameter	Value	Hyper-Parameter	Value	Hyper-Parameter	Value
n_estimators	79	n_estimators	974	n_estimators	331
max_depth	2	max_depth	10	max_depth	15
min_samples_split	6	learning_rate	0.92	learning_rate	0.93
max_leaf_nodes	18	colsample_bytree	0.56	colsample_bytree	0.69
random_state	14	subsample	0.97	subsample	0.04
		reg_alpha	9.59	reg_alpha	13.77
		reg_lambda	28.76	reg_lambda	43.31
		gamma	0.84	random_state	20
		random_state	15		

other algorithms, LGB uses a leaf-wise expansion, contributing to its fast learning speed. However, as a tree-based algorithm, it is prone to overfitting depending on the settings and unstable to handle a small number of features.

These three algorithms are ensemble learning algorithms that combine multiple decision trees to make predictions, providing robust generalization capability and predictive performance. Furthermore, prediction performance can be enhanced through hyperparameter tuning. In this study, for the improvement of the prediction model, hyperparameter tuning was performed using tree-based algorithms such as RF, XGB, and LGB. The training results of the models based on each algorithm are summarized in Table 6. When using normalized data, the R-square (R^2), the coefficient of determination for each algorithm is negative, indicating that the performance is not better than predicting the mean value. Root Mean Squared Error (RMSE) is a performance indicator that calculates the difference between predicted and actual values. A lower RMSE indicates better performance, and R^2 is an indicator of the accuracy of the prediction value, with values closer to 1 representing better performance.

4.2.2 Hyper-parameter tuning

In this study, hyperparameter tuning was attempted using normalized and standardized data. Hyperparameter tuning was performed using the validation data among the split data. Hyper-parameter tuning is a process of optimizing the parameters so that the prediction model with the algorithm achieves the highest performance. It was observed that models based on normalized data showed improved performance and Table 7 summarizes the R^2 values and RMSE values before and after hyperparameter tuning for each algorithm. For the normalized data, the training results of the models with hyperparameter tuning resulted in R^2 values above 0.9 from negative values. Also, the RMSE values were 0.0520, 0.0505, and 0.0314 for each algorithm in the predictive model after tuning. All algorithms improved model performance with the normalized data, while some did not with the standardized data. Therefore, normalized input data was used for machine learning, and the hyperparameters for each algorithm in the prediction model were summarized in Table 8.

Table 9 Performance evaluation metrics for each prediction model

	Random Forest	XGBoost	LightGBM
R^2	0.9390	0.9456	0.9782
RMSE	0.0520	0.0505	0.0314

The common hyperparameters for each algorithm are n_estimators and max_depth. The n_estimators parameter specifies the number of decision trees, determining the size of the ensemble. The max_depth parameter restricts the maximum depth of each decision tree, regulating the complexity of the model.

4.3 Evaluation of the prediction model

The test data was predicted using the prediction model derived from algorithm selection using training data and model optimization using validation data. Test data was not exposed to the algorithm during the training and validation processes to prevent overfitting. The results of predicting the settlement of the pile group in the final prediction model with hyperparameter tuning are summarized in Fig. 13.
As shown in Fig. 13(c), the distribution of predicted values is closer to the trend line in LGB than in RF and XGB. This means that the difference between the actual and predicted values is smaller in LGB. When calculating the minimum error of the settlement predicted by the prediction model, RF has an error of 0.0023mm, XGB has 0.0035mm, and LGB has 0.0002mm. RF and XGB both have 11.5% and 17.9% larger minimum errors than LGB. Furthermore, the maximum error of the prediction model is 8.95 mm, 8.33 mm, and 6.23 mm for each algorithm. RF and XGB have 0.44% and 0.34% larger minimum errors than LGB.

To evaluate the performance of the models predicted by each algorithm, R^2 and RMSE results are summarized in Table 9. The results indicate that LGB exhibits high performance, consistent with both training and validation outcomes. The tuned hyperparameter prediction model shows an R^2 of 0.9782 and an RMSE of 0.0314, with LGB outperforming other algorithms.

4.4 Analysis of the prediction model

In addition to evaluating the performance of the model, interpreting how variables impact predictions is crucial. For the tree models used in this study, the feature importance is a measure of how much each feature contributes to the segmentation of the tree. The feature importance is an indicator of how much each feature influenced the prediction in the process of predicting the target value. Fig. 14 shows the numerical value of feature importance for each prediction model. The sum of the importance scores of each independent variable is quantified based on 100 (%).

In Fig. 14, the influence of independent variables on the prediction model derived through each algorithm is summarized. P_N has the highest importance score at 65.04%, followed by P_{CTC} at 14.72%, E_{ref} at 11.53%, and P_L at 6.86%, while P_D and T_{CTC} showed minimal impact at

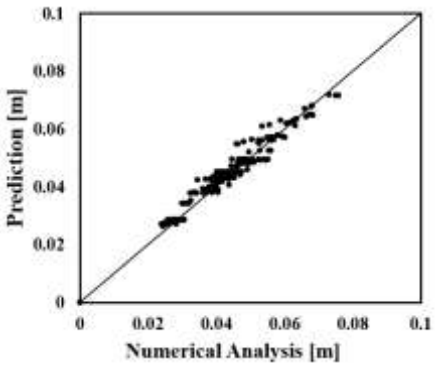

(a) Random Forest

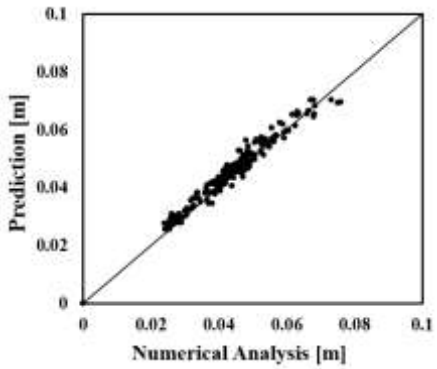

(b) XGBoost

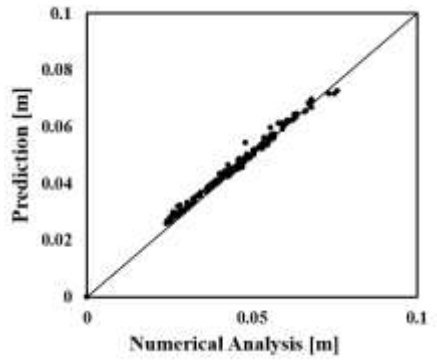

(c) LightGBM

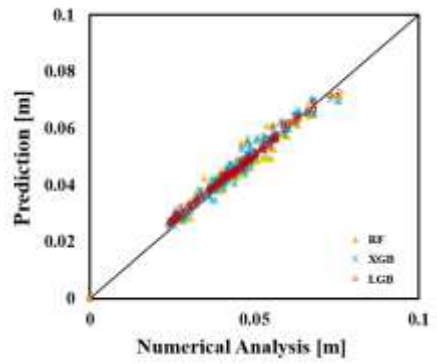

(d) Total

Fig. 13 Prediction of each algorithm

1.05% and 0.80%, respectively. Where, similar to RF, P_N has the most significant impact with a score of 64.81%. Unlike RF and XGB, the importance scores are relatively

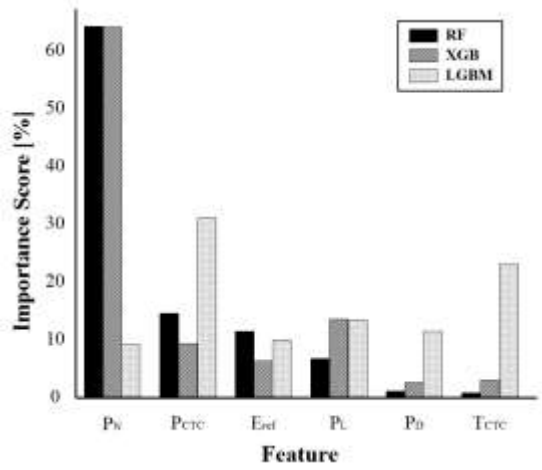

Fig. 14 Feature importance of each algorithm

Fig. 15 Correspondence between game theory and machine learning

evenly distributed. In the case of LGB, P_{CTC} holds the highest importance score at 31.32%, while P_N has the lowest importance score at 9.68%.

However, high feature importance does not provide information about whether it has a positive or negative impact on the prediction results. In other words, feature importance does not indicate the direction of influence. Additionally, the importance of variables should ideally remain consistent across models when using bagging or ensembles, but in practice, most feature importance measures show inconsistency.

To address these issues, Shapley Value can be used for analysis. The Shapley Value is a concept from the theory of fair distribution games, which is derived from how to fairly distribute the winnings among the players in a given game, and can correspond to as shown in Fig. 15. The Shapley Value remains consistent even when the model changes, allowing for the individual examination of how each feature influences the target value. Moreover, it offers the advantage of visualizing the impact of various combinations of variables.

Shapley Addictive exPlanation (SHAP) interprets the influence of each variable on individual predicted values additively, regardless of the model class, using Shapley Values. The impact of each variable on the prediction model through SHAP analysis is shown using the SHAP summary plot (Fig. 16). In the summary plot, a large absolute value of SHAP value means a large contribution to

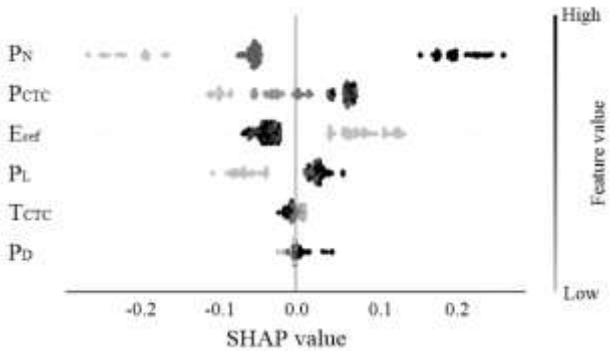

(a) Random Forest

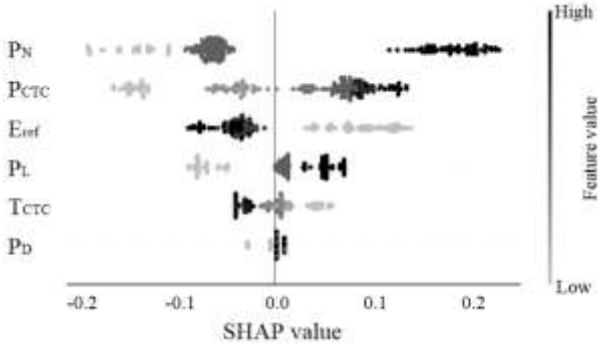

(b) XGBoost

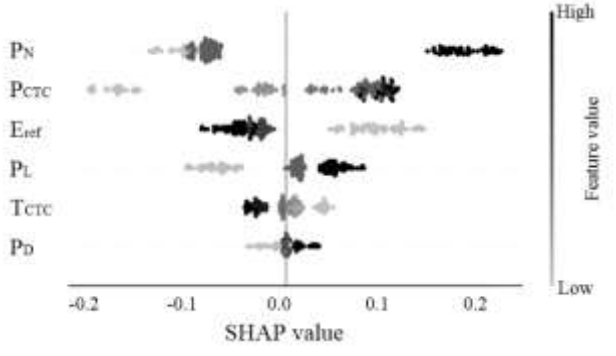

(c) LightGBM

Fig. 16 SHAP summary plot impacting the model output of each algorithm

the predicted value. If the feature contribution in the SHAP summary plot is positive, it means a positive effect compared to the average prediction, and conversely, if it is negative, it means a negative effect compared to the average prediction. SHAP Value is the average difference between the actual prediction and the average prediction for a given observation. Hence, while effective for prediction, caution should be exercised in attributing causality to the results.

Compared to Fig. 14, the summary plot (Fig. 16) shows that the feature importance does not depend on the algorithm applied to the model. feature importance for each algorithm is in the following order: P_N, P_{CTC}, E_{ref}, P_L, T_{CTC}, and P_D. In every model, P_N contributed the most to predicting pile group settlement. This means that a larger value of P_N contributes to a positive increase in the prediction of the model, i.e., the model predicts that the greater the number of piles, the greater the settlement of the pile group.

P_{CTC} is observed to have larger absolute SHAP Values for lower feature values. This indicates that a reduction in pile spacing has a substantial impact on pile group settlement. On the other hand, increasing the pile spacing seems to have a relatively lesser effect. Also, since the high feature value of P_{CTC} is positive, it can be predicted that the settlement increases as the pile spacing increases. This occurs because the vertical load is distributed, causing a reduction in the bearing capacity of the pile group as the pile spacing increases.

E_{ref} indicates that a high feature value is associated with a negative outcome, signifying that the model predicts a tendency for pile settlement to decrease as the modulus of elasticity of the ground increases. In addition, the absolute SHAP values are larger for the low feature value than for the high feature value, which means that the lower elastic modulus of the ground has a greater influence on the settlement of the pile group.

The distribution of SHAP Values in P_L and P_D shows that the settlement of the pile group increases as the length and diameter of the pile group increase. This suggests that, in isolation, the magnitude of the applied load increases with an increase in the length and diameter of the pile group. For T_{CTC}, the pile group settlement was found to be smaller as the tunnel spacing increased. However, T_{CTC} and P_D contributed less to the prediction of the pile group settlement compared to other features.

5. Conclusions

In this study, the behaviour of the pile group was investigated due to the excavation of a twin tunnel beneath an existing piled foundation in urban areas with limited infrastructure space, employing finite element numerical analysis based on laboratory model test results, was employed to examine the settlement of the pile group.

The numerical data obtained are utilized as input for the development of a machine-learning prediction model, and results can be drawn as below:

• The results of laboratory model tests generally indicated that settlements tend to decrease as the distance between tunnels increases. In Case I, the settlement was 30.2% larger than in Case II and 252.1% larger than in Case III.

• The numerical analysis reveals that various factors such as elastic modulus of the ground, pile diameter, pile length, number of piles, pile spacing, and tunnel spacing significantly influence pile group settlement. Unexpectedly, the settlement of the pile group increases with an increase in the number of piles, length, pile spacing, and diameter. This deviation from the conventional trend is attributed to the applied load variations and the absence of consideration for the raft effect of the pile group.

• A machine learning prediction model is developed and optimized using various algorithms, such as Random Forest, XGBoost, and LightGBM. Hyperparameter tuning is performed to enhance model performance, with normalized input data proving more effective. The prediction model, particularly with LGB, demonstrates high accuracy and outperforms other algorithms, as evidenced by the R^2 value of 0.9782 and the RMSE value of 0.0314.

• The analysis of feature importance in the prediction models reveals that P_N has the highest importance, at 65.04% for RF, 64.81% for XGB, and P_{CTC} is the highest at 31.32% for LGB. This shows that the contribution of the features to the prediction model is different for each algorithm. This is due to the inconsistency in the feature importance.

• To address these limitations, SHAP is utilized for prediction analysis, allowing for an additive interpretation of the impact of each variable. P_N consistently exerts the most significant influence on the prediction of pile group settlement in all models. Larger P_N values can be correlated with a positive increase in the settlement prediction.

• P_{CTC} demonstrates a substantial impact on settlement, with lower feature values resulting in larger SHAP values. This indicates that a reduction in pile spacing significantly influences the pile group settlement, while increased pile spacing has a relatively lesser effect.

In summary, the results from both laboratory model tests and numerical analysis revealed a reduction in ground displacement with varying pillar spacing in twin tunnels. However, upon further investigation through machine learning with additional variables, it was found that the number of piles has the most significant impact on ground displacement. Nevertheless, as this study is based on laboratory model testing, further research considering real field conditions is necessary. In future studies, we will explore the impact of additional independent variables on the behaviour of both the pile group and the ground through modelling that mimics real twin tunnelling scenarios.

Acknowledgments

This work was supported by the National Research Foundation of Korea (NRF) grant funded by the Korean government (MSIT) (No. 2021R1A2C2013162).

References

Ahn, C.Y., Park, D. and Moon, S.W. (2022), "Analysis of surface settlement troughs induced by twin shield tunnels in soil: A case study", *Geomech. Eng.*, **30**(4), 325-336. https://doi.org/10.12989/gae.2022.30.4.325.

Alseid, B., Chen, J., Huang, H. and Seo, H. (2023), "RCF machine learning method to measure for geological structures in 3d point cloud of rock tunnel face", Available at SSRN 4503641. http://dx.doi.org/10.2139/ssrn.4503641.

Ayasrah, M.M., Qiu, H. and Zhang, X. (2021), "Influence of cairo metro tunnel excavation on pile deep foundation of the adjacent underground structures: Numerical study", *Symmetry*, **13**(3), 426. https://doi.org/10.3390/sym13030426.

Chakeri, H., Hasanpour, R., Hindistan, M.A., and Ünver, B. (2011), "Analysis of interaction between tunnels in soft ground by 3D numerical modeling", *Bull. Eng. Geol. Environ.*, **70**, 439-448. https://doi.org/10.1007/s10064-010-0333-8.

Choi, J.I. and Lee, S.W. (2010), "Influence of existing tunnel on mechanical behavior of new tunnel", *KSCE J. Civil Eng.*, **14**,

773-783. https://doi.org/10.1007/s12205-010-1013-8.
Chu, B.L., Hsu, S.C., Chang, Y.L. and Lin, Y.S. (2007), "Mechanical behavior of a twin-tunnel in multi-layered formations", *Tunn. Undergr. Sp. Tech*., **22**(3), 351-362. https://doi.org/10.1016/j.tust.2006.06.003.
Das, B.M. (2011), Principles of Foundation Engineering, Cengage Learning, Boston, Massachusetts, USA.
Do, N.A., Dias, D. and Oreste, P. (2016), "3D numerical investigation of mechanized twin tunnels in soft ground–Influence of lagging distance between two tunnel faces", *Eng. Struct*., **109**, 117-125. https://doi.org/10.1016/j.engstruct.2015.11.053.
Fang, Q., Zhang, D., Li, Q. and Wong, L.N.Y. (2015), "Effects of twin tunnels construction beneath existing shield-driven twin tunnels", *Tunn. Undergr. Sp. Tech*., **45**, 128-137. https://doi.org/10.1016/j.tust.2014.10.001.
Gordan, B., Koopialipoor, M., Clementking, A., Tootoonchi, H., and Tonnizam Mohamad, E. (2019), "Estimating and optimizing safety factors of retaining wall through neural network and bee colony techniques", *Eng. with Compu*t., **35**, 945-954. https://doi.org/10.1007/s00366-018-0642-2.
Han, Y., Jiang, X., Wang, Y. and Wang, H. (2023), "Usage of coot optimization-based random forests analysis for determining the shallow foundation settlement", *Geomech. Eng*., **32**(3), 271-291. https://doi.org/10.12989/gae.2023.32.3.271.
Heama, N., Jongpradist, P., Lueprasert, P. and Suwansawat, S. (2017), "Investigation on tunnel responses due to adjacent loaded pile by 3D finite element analysis", *Geomate J*., **12**(31), 63-70. https://doi.org/10.21660/2017.31.6542.
Hong, S.K., Oh, D.W., Kong, S.M. and Lee, Y.J. (2020), "Investigation of divergence tunnel excavation according to horizontal offsets between tunnels", *Geomech. Eng*., **21**(2), 111-122. https://doi.org/10.12989/gae.2020.21.2.111.
Jeon, Y.J. and Lee, C.J. (2023), "Analysis of pile group behaviour to adjacent tunnelling considering ground reinforcement conditions with assessment of stability of superstructures", *Geomech. Eng*., **33**(5), 463-475. https://doi.org/10.12989/gae.2023.33.5.463.
Jung, H.S., Kim, J.H., Yoon, H.H., Sagong, M. and Lee, H.H. (2022), "Experimental study to determine the optimal tensile force of non-open cut tunnels using concrete modular roof method", *Geomech. Eng*., **29**(3), 229-236. https://doi.org/10.12989/gae.2022.29.3.229.
Kim, C.Y., Bae, G.J., Hong, S.W., Park, C.H., Moon, H.K. and Shin, H.S. (2001), "Neural network based prediction of ground surface settlements due to tunnelling", *Comput. Geotech*., **28**(6-7), 517-547. https://doi.org/10.1016/S0266-352X(01)00011-8.
Kim, Y.S., Ko, H.W., Kim, J.H. and Lee, J.G. (2012), "Dynamic deformation characteristics of Joomunjin standard sand using cyclic triaxial test", *J. Korean Geotech. Soc*., **28**(12), 53-64. https://doi.org/10.7843/kgs.2012.28.12.53.
Kong, S.M., Jung, H.S. and Lee, Y.J. (2017), "Investigation of ground behaviour adjacent to an embedded pile according to various tunnel volume losses", *Int. J. Geo-Eng*., **8**, 1-15. https://doi.org/10.1186/s40703-017-0043-1.
Kong, S.M., Oh, D.W., Ahn, H.Y., Lee, H.G. and Lee, Y.J. (2016), "Investigation of ground behaviour between plane-strain grouped pile and 2-arch tunnel station excavation", *J. Korean Tunn. Undergr. Sp. Assoc*., **18**(6), 535-544. https://doi.org/10.9711/KTAJ.2016.18.6.535.
Korean Geotechnical Society (2016), Design Criteria for Structure Foundation, Korean Geotechnical Society, Seoul, Republic of Korea.
Lambe, T.W. and Whitman, R.V. (1979), Soil mechanics, John Wiley & Son, Hoboken, New Jersey, USA.
Liu, X., Suliman, L., Zhou, X., Zhang, J., Xu, B., Xiong, F. and Abd Elmageed, A. (2022), "The difference in the slope supported system when excavating twin tunnels: Model test and numerical simulation", *Geomech. Eng*., **31**(1), 15-30. https://doi.org/10.12989/gae.2022.31.1.015.
Marshall, A.M. and Haji, T. (2015), "An analytical study of tunnel–pile interaction", *Tunn. Undergr. Sp. Tech*., **45**, 43-51. https://doi.org/10.1016/j.tust.2014.09.001.
Mirhabibi, A. and Soroush, A. (2012), "Effects of surface buildings on twin tunnelling-induced ground settlements", *Tunn. Undergr. Sp. Tech*., **29**, 40-51. https://doi.org/10.1016/j.tust.2011.12.009.
Mroueh, H., and Shahrour, I. (2002), "Three-dimensional finite element analysis of the interaction between tunneling and pile foundations", *Int. J. Numer. Anal. Method. Geomech*., **26**(3), 217-230. https://doi.org/10.1002/nag.194.
Nejad, F.P., Jaksa, M.B., Kakhi, M. and McCabe, B.A. (2009), "Prediction of pile settlement using artificial neural networks based on standard penetration test data", *Comput. Geotech*., **36**(7), 1125-1133. https://doi.org/10.1016/j.compgeo.2009.04.003.
Ng, C.W.W. and Lu, H. (2014), "Effects of the construction sequence of twin tunnels at different depths on an existing pile", *Can. Geotech. J.*, **51**(2), 173-183. https://doi.org/10.1139/cgj-2012-0452.
Ng, C.W.W., Lu, H. and Peng, S.Y. (2013), "Three-dimensional centrifuge modelling of the effects of twin tunnelling on an existing pile", *Tunn. Undergr. Sp. Tech*., **35**, 189-199. https://doi.org/10.1016/j.tust.2012.07.008.
Oh, D.W., Kong, S.M., Kim, S.B. and Lee, Y.J. (2023), "Prediction and analysis of axial stress of piles for piled raft due to adjacent tunneling using explainable AI", *Appl. Sci*., **13**(10), 6074. https://doi.org/10.3390/app13106074.
Oh, D.W., Kong, S.M., Lee, Y.J. and Park, H.J. (2021), "Prediction of change rate of settlement for piled raft due to adjacent tunneling using machine learning", *Appl. Sci*., **11**(13), 6009. https://doi.org/10.3390/app11136009.
PLXIS (2023), Manuals-PLAXIS; Bentley Systems, Pennsylvania, USA. https://communities.bentley.com/products/geotech-analysis/w/wiki/46137/manuals---plaxis
Potts, D.M. and Zdravkovic, L. (2001), Finite Element Analysis in Geotechnical Engineering: Application, Thomas Telford, London, United Kingdom.
Sou-Sen, L. and Hsien-Chuang, L. (2004), "Neural-network-based regression model of ground surface settlement induced by deep excavation", *Automat. Constr*., **13**(3), 279-289. https://doi.org/10.1016/S0926-5805(03)00018-9.
Xiang, Y. and Feng, S. (2013), "Theoretical prediction of the potential plastic zone of shallow tunneling in vicinity of pile foundation in soils", *Tunn. Undergr. Sp. Tech*., **38**, 115-121. https://doi.org/10.1016/j.tust.2013.05.006.